Characterization and validation of next generation image sensors for space applications

Nicholas R. Shade*[a,b], Gillian Kyne[b], Shouleh Nikzad*[b], Edoardo Charbon[c], Eric R. Fossum[a]
[a]Dartmouth College, 15 Thayer Drive, Hanover, NH, USA 03755; [b]Jet Propulsion Laboratory, California Institute of Technology; [c]EPFL

ABSTRACT

Astronomers are always looking to image fainter and farther objects in the night sky. Recent improvements in signal to noise ratio in solid-state detector technology have the potential to provide researchers with the ability to determine photon-number including single photons, allowing them to sense at the limit of physics. The quanta image sensor (QIS), the electron-multiplying charge-coupled device (EMCCD), and the single-photon avalanche diode (SPAD) are three types of next-generation silicon detectors that can capture images with high sensitivity and low input-referred read noise that can result in the ability to count photons. QIS uses a unique CMOS pixel topology that increases conversion gain without impact ionization, reducing readout noise to deep-sub-electron levels and enabling photon-number resolution, high dynamic range, and high spatial resolution. The EMCCD uses a CCD sensor design that amplifies the signal a small amount but very high number of times during readout using impact ionization, reducing readout noise to deep-sub-electron levels and a degree of photon-number resolution. SPAD uses fast in-pixel signal amplification using impact ionization and positive feedback to achieve negligible read noise and is capable of measuring the precise time-of-arrival of photons, enabling high-precision distance measurement and photon-counting. A representative device of each technology was characterized and evaluated with space flight missions in mind. Additionally, a variety of CCD and CMOS image sensors with "Skipper" readout are being explored for photon-number-resolving applications by several groups, including parts of our team, and we will also briefly discuss the Skipper approach in this report. Additionally, recommendations for potential improvements of the technology to better support the astronomical community are made.

Keywords: CIS, QIS, SPAD, EMCCD, Image Sensor, photon counting, photon-number

INTRODUCTION

While the idea of photon-counting image sensors (single-photon and photon-number resolving) is not new, only recently have solid-state photon-counting detectors started being widely available for commercial and scientific use [1]. Next-generation sensors are designed to detect individual photons, the fundamental particles or quanta of light, which allows for highly sensitive measurements that are crucial in astronomy. Advances in technology have led to significant improvements in the performance of photon-counting sensors, enabling astronomers to observe phenomena that were once beyond the practical reach of traditional imaging methods.

Photon-counting sensors come in various forms, each with unique characteristics that make them suitable for different aspects of astronomical observation. Common types of photon-counting sensors include image-tube based technologies such as photomultiplier tubes (PMTs) and microchannel plates (MCPs), single-photon avalanche diodes (SPADs), superconducting nanowire single-photon detectors (SNSPDs), transition edge sensors (TES), quanta image sensors (QIS), and electron-multiplying charge-coupled devices (EMCCD) ([2] – [3]). These sensors vary in their operational principles, spectral range, and the environments in which they can be used effectively. In addition to unique sensor topologies to allow for photon-counting, there has been a recent push in enhancements of the readout that allows for photon-counting through multiple-sample-readout methodologies [4].

This report aims to provide a comprehensive overview of the different types of next generation photon-counting sensors, their respective operational principles, and their applications in astronomy investigate the various technical aspects needed for future space flight missions. Of note is the increased desire to create new large-format telescopes in the UV/Visible/NIR range as described in the Astro2020 decadal survey [5]. Additionally, the general technological merits of the various photon-counting image sensor systems will be explored. The report will conclude with a focused preliminary experimental investigation into the silicon-based sensors (EMCCD, SPAD, and QIS) due to their ability to be easily enhanced for various wavelengths of sensitivity ([6] and [7]). By understanding the capabilities and limitations of these sensors, we hope to continue to push the boundaries of astronomical research and deepen our understanding of the universe.

*nicholas.r.shade.th@dartmouth.edu, engineering.dartmouth.edu; shouleh.nikzad@jpl.nasa.gov, jpl.nasa.gov

X-Ray, Optical, and Infrared Detectors for Astronomy XI, edited by Andrew D. Holland, Kyriaki Minoglou, Proc. of SPIE Vol. 13103, 131030U · © 2024 SPIE
0277-786X · doi: 10.1117/12.3021522

APPLICATIONS IN ASTRONOMY

Photon-counting sensors are quickly becoming integral to a multitude of astronomical applications. Their ability to accurately detect photons makes them invaluable for deep-space observation. In spectroscopy, these sensors provide high-resolution data, allowing astronomers to determine the composition, temperature, and movement of celestial bodies. Time-resolved astronomy benefits from the precise timing capabilities of photon-counting sensors, enabling the study of transient events like supernovae and gamma-ray bursts. Additionally, the search for and characterization of exoplanets utilizes the sensitivity of these sensors to detect minute changes in starlight as planets transit their host stars or detect ultra-faint signal from the planet after starlight suppression [8]. Below, table 1 lists some key performance metrics along with a description and importance of the metric.

Table 1. Overview of Important Camera Features

Specification	Description	Importance
Resolution	Number of pixels in the camera sensor.	Higher resolution allows capturing more detail in celestial objects.
Pixel Size	Size of each pixel in micrometers (μm).	Smaller pixels can allow higher resolution, but larger pixels are better for low-light conditions.
Quantum Efficiency	Percentage of photons incident on the sensor that are converted into electrons.	Higher quantum efficiency means better sensitivity to faint light from distant object.
Read Noise	Input-referred noise generated by the camera's electronics when reading the signal.	Lower read noise can improve the quality of images, especially in low-light conditions.
Full-Well Capacity	Maximum number of electrons a pixel can hold before saturating.	Higher capacity allows capturing brighter objects without saturation.
Linear Dynamic Range	Ratio between the largest and smallest measurable light intensities over a linear regime.	Higher dynamic range helps in capturing both very bright and very faint objects in the same image.
Cooling	Requirement to cool the camera sensor to reduce thermal noise and improve image.	Cooling is crucial for long exposures needed in deep-sky astrophotography.
Frame Rate	Number of frames the camera can capture per second.	Higher frame rates are important for capturing fast-moving objects like planets.
Bit Depth	Number of bits used to meaningfully represent each pixel's intensity.	Higher bit depth allows capturing more subtle variations in light intensity.

While all these metrics are important for every image sensor, many of the imaging performance metrics compete with each other and there is currently no way to create a sensor that is optimal across the whole performance spectrum. This results in astronomers making trade-offs and prioritizing the different criteria and sensors based on different scientific objectives and experiments. The prioritization of different sensor requirements can be seen below in table 2, which lists some examples of future missions and the corresponding image sensor requirement most relevant to it.

Table 2: Sample Mission Specific Camera Requirements

Mission	Launch Date	Image Sensor Requirements
Artemis II	September 2025	High-resolution, low-light sensors for capturing detailed images of the Moon's surface. [9]
SPHEREx	2025	Hyperspectral imaging sensors, covering a wide range of wavelengths from visible to near-infrared. [10]
Dragonfly	2028	Multispectral cameras and LIDAR for surface mapping. [11]
Ariel	2029	Infrared sensors with high dynamic range for studying exoplanet atmospheres. [12]
Comet Interceptor	2029	High-speed, high-resolution sensors for capturing fast-moving comet details. [13]

While imaging detectors overall have been able to meet the challenges put forth by the goals of future space missions, no singular piece of technology created has met every technological challenge simultaneously. There is constantly a push and a pull by the science and engineering teams on which parameters really matter to reach science objectives and which technologies can meet those needs. The cutting edge of science missions also has to deal with technology readiness level issues related to selecting the most advanced imaging sensors that do not have the heritage and proven track record that some of the others might have.

OVERVIEW OF SINGLE-PHOTON AND PHOTON-NUMBER RESOLVING SENSORS

As discussed, single-photon and photon-number resolving imaging sensors are available in various technology types which leads to use-dependent based performance benefits. To achieve such sensitivity, the sensors use high gain following photoelectron generation to overcome downstream readout circuit noise and thus achieve deep-sub-electron input-referred read noise. SPADs use Geiger mode diode areas to create digital pulses of photon arrivals [3]. SNSPDs uses cryogenic nanowires to detect charge and are known for their high detection efficiency and low timing jitter [14]. TESs leverage the sharp change in resistance near the superconducting transition to detect single photons, offering high energy resolution and photon-number resolving capabilities. EMCCDs are highly sensitive detectors used in low-light imaging applications, capable of detecting single photons with low noise. PMTs despite being older technology, are still used in some applications due to their spectral sensitivity. MCPs are also used due to their spectral sensitivity in wavelengths that silicon detectors do not excel at such as UV. QIS sensors are the newest and use high conversion gain pixels in order to detect low light levels. In space imaging applications, all of these sensors are particularly valuable. SNSPDs and TESs are used in astronomical observations, space-based LIDAR systems, and optical communications, providing high sensitivity and precision for detecting faint light from distant celestial objects. EMCCDs are employed in space telescopes and satellites to capture high-resolution images of stars, galaxies, and other astronomical phenomena. SPAD have been used for development of in situ spectroscopy such as Raman, enabling delineation of Raman signal from fluorescence background.

While all of these technologies have their current use cases, the SPAD, QIS, and EMCCD are currently viewed by many as important technologies to continue to develop due to their theoretically higher performance ceiling. These devices operate closest to traditional image sensors which allows greater flexibility in how they can be used. Additionally, since they are manufactured using well-known and well-studied silicon substrates, there are various ways to enhance their performance using surface treatments and multi-layered coatings, agnostic to architecture, to apply filters or to extend the spectral sensitivity [6].

OPERATIONAL PRINCIPLES OF SELECTED PHOTON-COUNTING SENSORS

While at the most basic operational level, the selected sensors are based on the photoelectric effect, where photons striking a photosensitive material can liberate electrons or holes in the form of charge carriers. These charge carriers are then converted to a voltage and processed into a digital signal. However, how each sensor applies gain to the initial low-level signal varies significantly. The readout of the then gained signal is also different for the different camera types.

EMCCD Operation

EMCCDs are an enhancement of the traditional CCD. Traditional CCDs have a series of photosensitive and non-photosensitive gates that transfer charge in parallel to a series register that then goes to a single readout amplifier that converts the charge carriers to a voltage. In 2001, Hynecek at Texas Instruments invented the “Impactron” which would later become known as the EMCCD. He discovered that by altering the standard operation of CCD by creating a high field area of the sensor, nearly noiseless gain can be applied to the charge packets [15]. It is now typical for EMCCDs to include an additional multiplication register before the standard charge-to-voltage amplifier. In the multiplication register, the clocking voltage is dramatically increased from the standard operating clocking voltage, for example from 5 V to 40 V. This causes a high electric field between clock phases over a short distance yielding a small probability of impact ionization, e.g., 1%, which results in a concomitant increase in the number of carriers when repeated over many transfer stages. With enough transfers through the multiplication register, a total amplification in the order of 1000-fold is achievable. The main drawback of these sensors is the need for cooling (typically -75 to -100 °C) to reduce dark current (which is also amplified) and achieve acceptable levels of read noise [16].

SPAD Operation

SPADs cameras are semiconductor devices that operate in a high voltage mode above the breakdown threshold known as Geiger mode. When a photon is absorbed by the semiconductor, it generates an electron-hole pair (EHP). If this occurs in a (high) field region, or one or both carriers diffuse to a high-field region, the charge carriers (electron and/or hole) gain kinetic energy and travel in opposite directions. If a carrier with increased energy, above some threshold, interacts with the lattice it will create additional electron-hole pairs in a process known as impact ionization. The original carrier and any

additional electron-hole pairs will then be re-energized if they remain in the high electric field region and they will further create additional charge carriers. This exponential process is known as avalanche multiplication and can include positive feedback if both types of carriers are involved since the electrons and holes travel in opposite directions. This results in a significant and measurable current pulse from a single absorbed photon. Due to the fast and high gain of avalanche multiplication, SPAD cameras can be used for precise timing measurements since they can always be reading out signal and not limited by integration-time uncertainty. However, while a SPAD pixel is in active avalanche, additional photons will not create a meaningful difference in the resultant signal level due to the presence of so many additional charge carriers from the avalanche process and photon arrival cannot be resolved during this period. To reset the pixels to sense new photons, the avalanche process needs to be quenched. This is an active or passive process that reduces the voltage across the SPAD stopping or "quenching" the multiplication process. The choice of active or passive quenching depends on speed, power, or complexity requirements. This causes the main limitation of the SPADs in that due to the need for quenching, there are periods where the device "misses" photoelectrons in which is known as the deadtime of the pixel [17].

QIS Operation

QIS cameras are different from standard CMOS image sensors in that they use a unique CMOS pixel topology. Created at Dartmouth, Fossum and his research group figured out a way to create a very high charge to voltage conversion gain pixel using a tiny capacitor. While the use of a pinned-photodiode, common in scientific CMOS image sensors, is possible, to achieve small pixel size a vertically-based backside-illuminated pixel with a buried storage well was developed. A pump-gate is used to transfer the signal electron(s) to the ultra-low capacitance sense node for readout. The resulting capacitance from this new topology can be quite small which allows for very high conversion gain and signal amplification without the need for impact ionization and the associated high-voltage operation. These improvements allow QIS devices to work at room temperature with very low dark current and much lower power consumption than the other technologies [18]. The main drawback of QIS devices is residual non-uniformity of the quantizer threshold voltage or ADC; however, there have been several proposals to mitigate this issue [19].

Skipper Operation

Additionally, multi-sample-readout has been shown as a viable alternative to developing unique pixel topologies to increase the performance of standard CCDs and CIS cameras [20]. "Skipper" readout operates in a similar way to correlated multi-sampling (CMS) in that many readouts of the reset and signal level are averaged together. The difference is that CMS takes multiple samples of the reset level and then takes multiple samples of the signal level. This causes correlation between the respective samples of each level which allows the averaging to reduce the final noise in the signal. In Skipper readout the signal charge is moved back and forth between the sense node and a storage node many times. Therefore, each sample of the reset level and signal level are independent events, but the noise between a reset and a sample is more highly correlated together than in CMS allowing the use of correlated double sampling (CDS) to suppress kTC noise. This leads to more noise in each set of samples; however, it increases the signal to noise ratio by a higher rate since the higher correlation allows the noise to be averaged away more thoroughly and thus improving imaging performance [4].

Each of these sensors has its own set of advantages and limitations, which are considered when selecting the appropriate sensor for a particular astronomical application. The choice of sensor depends on factors such as the wavelength of interest, the required sensitivity, the environmental conditions, timing needs, and the specific scientific goals of the observation. In the following sections, we will explore the applications of these photon-counting sensors in greater detail, highlighting their contributions to astronomy.

CHARACTERIZATION OF QIS, EMCCD, AND SPAD

A full characterization plan was developed to test all three camera technologies on a unified testing apparatus. This plan involved acquiring a QIS camera, EMCCD camera, and a SPAD camera from various collaborators. Those cameras would then be tested at NASA-JPL utilizing a vacuum-enabled UV/VIS monochromator setup. This allows for very high precision measurements to be taken at various wavelengths extending into the far UV spectrum. Standard photon transfer curve (PTC) graphs would be used as the baseline for traditional noise, gain, and full well analysis. The photon-counting histogram (PCH) also calculates read noise and conversion gain but based on a single photon flux measurement rather than a sweep of intensities. The PCH method is especially useful for its efficiency in testing variations across the whole image sensor by providing per pixel performance characterization [21]. Quantum efficiency (QE) measures whole camera system performance by measuring photon detection effectiveness. The QE curves would be taken across the visible and UV

wavelength spectrum based on the PCH methodology. Finally, dark current (or dark count rate in the case of the SPAD) would be measured to help evaluate the need for cooling of the sensors and how long the cameras can integrate a single before becoming too corrupted with spurious data.

However, this plan was not able to be fully realized at this time due to various external factors and complications. The QIS camera was able to be most thoroughly tested which is important because it is the least well studied technology. The results for the EMCCD and SPAD camera was supplemented by standard published figures where the results could not be taken.

EMCCD Results

The EMCCD tested for this project is a delta-doped Teledyne-e2v CCD201-20 [7]. It was further enhanced with custom 5-layer anti-reflection coating with processing carried out at NASA-JPL (presented at this conference). This shows the flexibility of silicon sensors in that they can be augmented by well-studied coating techniques. The EMCCD can be operated with and without the EM gain. Without the EM gain the resulting PTC is shown in figure 1. This graph shows a good shot-noise-limited signal. Due to time constraints and subsequent testing limitations, the PTC graph was not plotted until the noise peaked and roll-off was observed to indicate full well capacity. The result is still valuable in that it shows the sensor exhibiting the expected shot noise limited slope in the linear region. It also shows the expected tail to read noise limited signal in the left-hand portion of the graph.

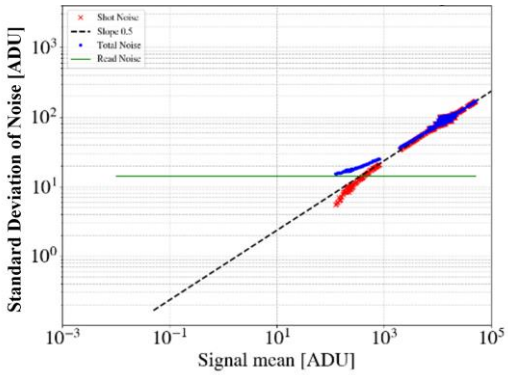

Figure 1. PTC of EMCCD camera without the high voltage gain. Taken at -90 °C with a constant 525 nm light source and the integration time as the variable. [1 ADU ~ 1 e^-].

When utilizing the EM gain the new PTC is shown in figure 2. The measured gain is 1290. This graph also exhibits expected shot noise limited signal. The measured noise floor is higher than without the EM gain, which indicates there is room for improvement of the clock timings and voltages.

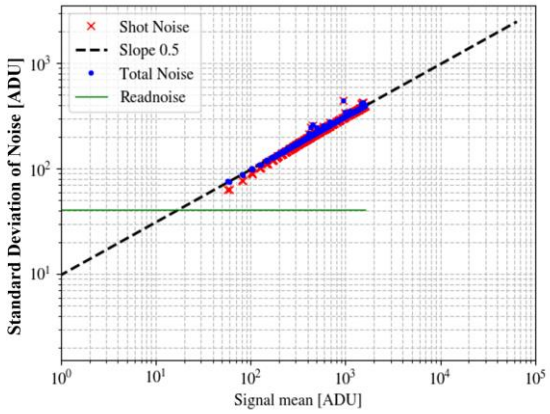

Figure 2. PTC for the EMCCD with the EM gain active at a 1290 times multiplier. It was performed at -90 °C with 525 nm light.

The QE performance of a detector is a complex function that is related to the semiconductor design and manufacturing of the sensor, the coatings and backside treatment of the sensor, and the optics on top of the sensor. For back illuminated silicon detectors, regardless of pixel architecture, 2D doping (encompassing delta doping and superlattice doping) provides stable, reflection limited response for silicon detectors. Coating treatments further allow scientists and engineers to selectively increase or decrease the QE of the sensors. This allows them to choose to either boost the sensor performance across the whole desired spectrum, or they can choose to specifically tailor detectors to only in the wavelengths that they need for their science experiments. This means QE results tend to be very mission dependent. An example of general performance boosting is shown in figure 3 which also shows the before and after performance improvement of the sensor. In comparison, two examples of the tailorable nature of coating treatments of 2D-doped detectors are shown in figure 4. The left hand graph was performed on a device with a 5-layer anti-reflection coating. The results have been mission enabling for Faint Intergalactic Redshifted Emission Balloon experiment (FIREBall-2) and Star-Planet Activity Research CubeSat (SPARCS) missions. Additionally, the right hand graph (presented at this conference by Jewell [22]) shows the ability to take the same sensor and tailor its wavelength response to achieve different science objectives.

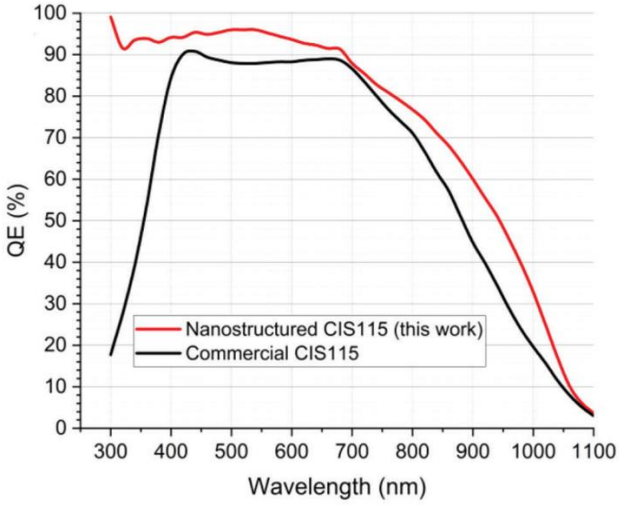

Figure 3: "QE of the nanostructured CIS115 compared to the commercial CIS115 device" from [23].

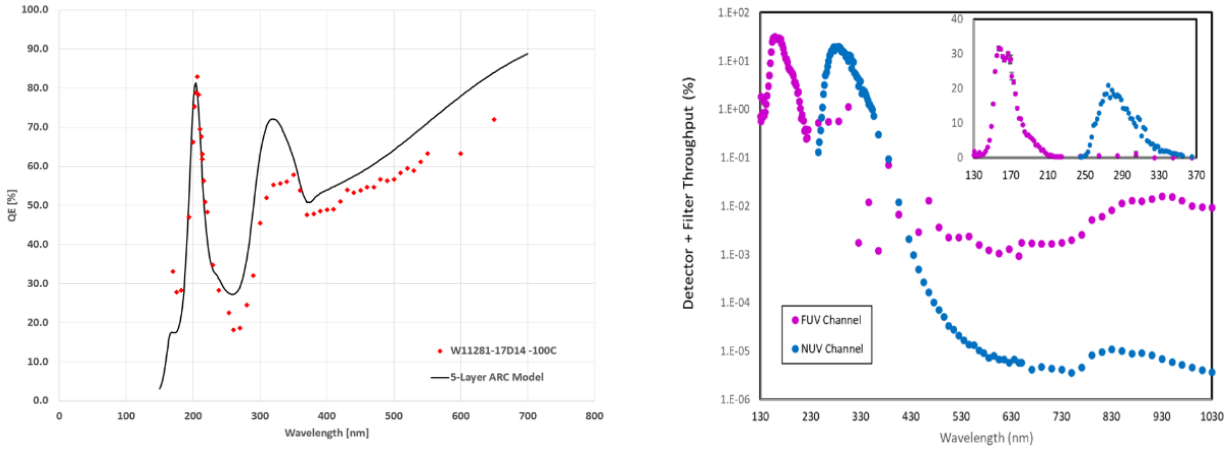

Figure 4. LHS: Quantum efficiency vs. wavelength plot for a 5-layer coating deposited on a thinned, delta-doped Te2v CCD201-20 for the FIREBall-2 mission. The peak QE is 67.6% at 206 nm and the data has been corrected using conversion gain measurements from photon transfer curves at each wavelength from [24]. RHS: The Star-Planet Activity Research CubeSat (SPARCS) detector for both NUV (blue) and FUV (magenta) channels offer high in-band performance with several orders of magnitude out-of-band rejection (presented by Jewell at JPL in this conference). All detector characterization was performed at JPL using a 1-m vacuum UV/VIS monochromator.

SPAD Results

Due to manufacturing delays, new SPAD data was not able to be captured in time for presentation and publication. However, there are results from other prior publications that are available and can be used for comparison. Additional data will be acquired once the camera is received. Comparison against prior reported figures will also be completed.

First, [25] contains figure 5 which shows the photon detection probability (PDP) of the SwissSPAD2 camera from EPFL. Photon detection probability is used to qualify SPAD cameras since it considers both quantum efficiency and dead time of the sensor which both together influence light gathering ability of SPAD cameras. For a device with limited surface enhancements, it exhibits good performance as seen in figure 5. Further tests with NASA-JPL's custom surface treatments will provide valuable insight into how well performance can be improved.

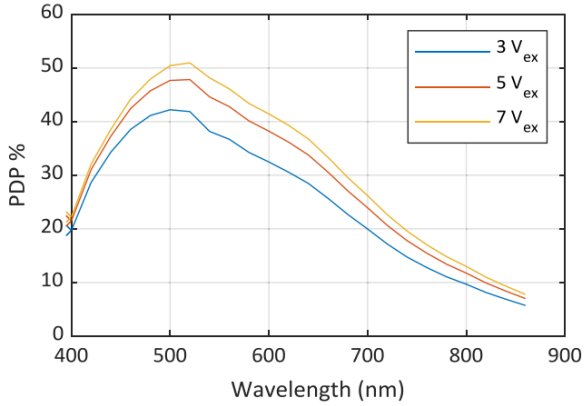

Figure 5. Graph of photon detection probability with the SPAD camera taken from [25].

Due to the nature of SPAD cameras, dark count rate (DCR) is used instead of dark current. Both metrics use the same units of electron per second, but DCR is more accurate for SPAD cameras due to their dead time period where measurement information is lost. Figure 6 shows the dark count rate of the SPAD camera for various operating conditions.

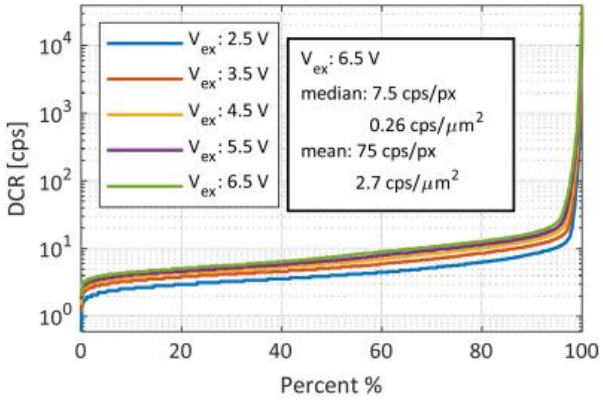

Figure 6. Graph of the cumulative distribution of the dark count rate of the SPAD camera taken from [25].

Comparing figures 5 and 6 shows an important characteristic of SPAD cameras. The overvoltage of the camera is a tunable parameter, but there is no strict optimal value for the overvoltage since generally increase overvoltage improves PDP but negatively impacts DCR. Instead, the overvoltage needs to be optimized based on the use case operating requirements to find an acceptable balance between PDP and DCR.

QIS Results

The primary QIS camera tested is an early Gigajot production camera. Overall, from a user perspective it operates the same as a traditional CMOS camera, but with much improved performance. The standard operation of the camera was to

use a light-controlled system to block outside light and an LED array to provide a flat-field photon flux. The camera actively cools itself to 10 °C. The camera was programmed to use eight CMS cycles.

A standard PTC graph of the camera is shown in figure 7. It was captured using 15 steps of integration time from the minimum to the maximum integration time with a 300 nm light source. The resulting plot exhibits the noise floor of the sensor on the left portion of the graph before becoming very linear in the shot noise limited region, as expected.

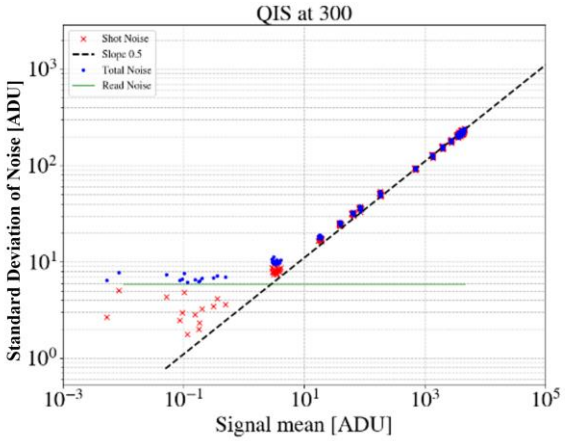

Figure 7. Graph of photon transfer curve of QIS camera. Taken at 10 °C with a constant 300 nm light source and the integration time as the variable. [1 ADU = 0.083 e^-].

As previously described, the uniformity of the QIS camera is one of its limitations. This can be seen in figure 8 through 10 when looking at the per pixel conversion gain. The PCH testing setup uses LED diodes that are shown into one port of an integration sphere. The output of the integration sphere then goes through a 20nm FWHM band pass filter at the corresponding wavelength. The flat field light then goes right onto the image sensor without a lens. 10,000 frames were then captured for analysis as described in [21]. As seen in the charts there is some pixel-to-pixel variation in the noise performance due to 1/f noise in the source follower and conversion gain variation; however, the peak of the curve is at 0.350 e^- which is about sufficient for reliable photon-counting [26], although lower noise is desired [27]. The conversion gain is also relatively high at about 12 DN/e-. While the exact values are not stated, from previous work QIS cameras generally use a least significant bit of around 200 µV/DN with an 8x amplifier gain. This would result in an approximate 300 µV/e- conversion gain.

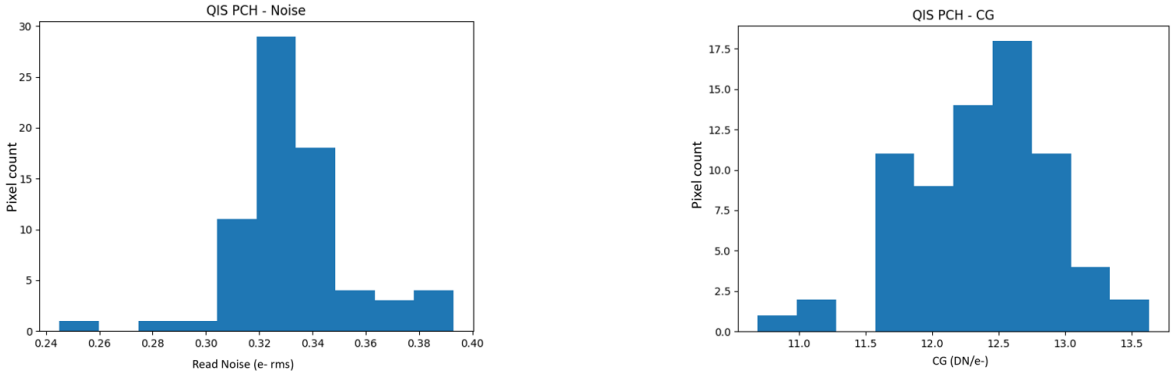

Figure 8. Graphs of the results of the photon-counting histogram algorithm for the QIS camera at 265 nm. Left is the graph of the individual pixel noise values. Right is the graph of the per pixel conversion gain values.

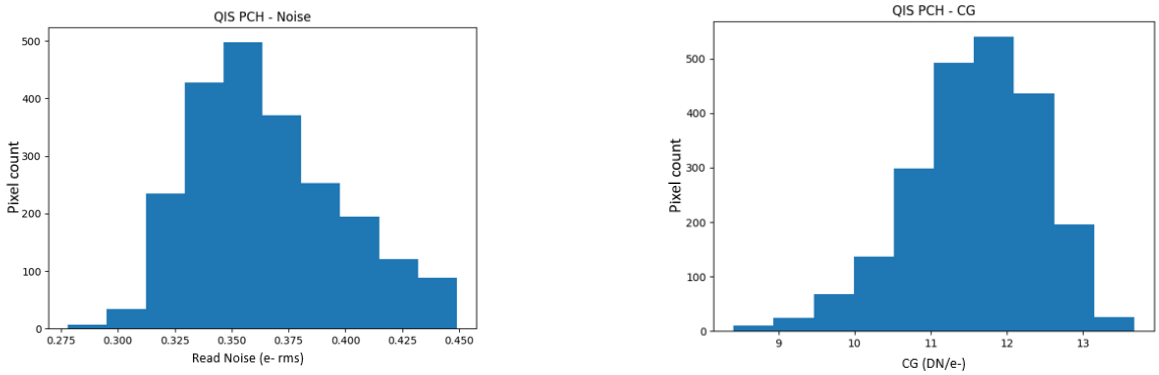

Figure 9. Graphs of the results of the photon-counting histogram algorithm for the QIS camera at 300 nm. Left is the graph of the individual pixel noise values. Right is the graph of the per pixel conversion gain values.

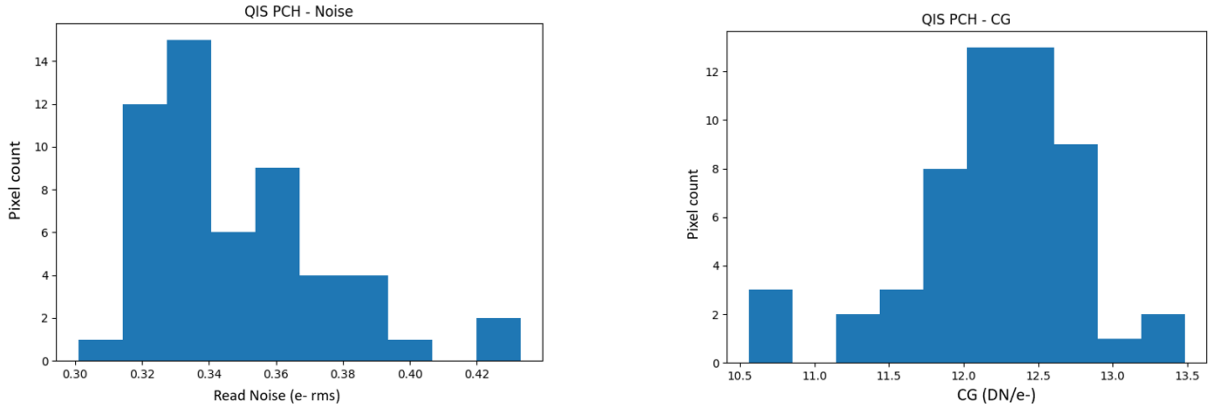

Figure 10. Graphs of the results of the photon-counting histogram algorithm for the QIS camera at 405 nm. Left is the graph of the individual pixel noise values. Right is the graph of the per pixel conversion gain values.

The dark current analysis graph is shown in figure 11. Using 20 logarithmic steps from the shortest (64 µs) to the longest (4.9 s) integration time, 100 frames of data was collected at each step. To process the data the mean pixel value at each integration time was calculated. Those values were then plotted against integration time. Taking the slope of the resulting plot yields the dark current value for the camera. The resulting plot is very linear which is expected and has a slope of 0.57 e^-/s.

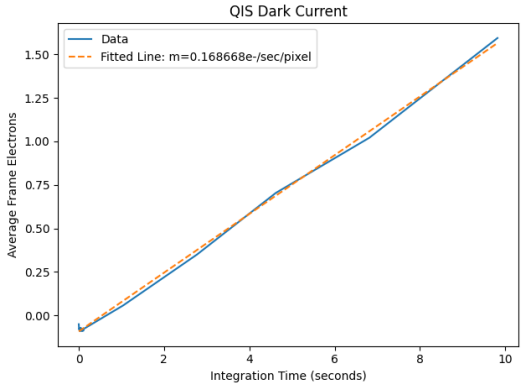

Figure 11. Graph of QIS dark current. Taken at 10 °C.

Overall, the various other parameters of the sensors are best summarized in a table. The table further shows that each camera has its own merits beyond what can be empirically assessed [28]. The most notable parameters are power usage, and resolution. Not shown on the table is the ability to determine precise distance information which is best achieved by the SPAD cameras.

Table 3. High-Level Summary of Various Photon-Counting Detector Architectures (recreated from [28]). More work is underway for further comparisons finer assignments of parameters for these technologies.

	QIS	EMCCD	SPAD
Single-Photon Sensitivity	Yes	Yes, with cooling	Yes
Photon Number Resolution	Yes	No	No
Dark Current	Low	High	High
Pixel Size	Small	Large	Large
Pixel Resolution	High	Low	Low
Quantum Efficiency	High	High	Low
Power	Low	High	High
System Simplicity	High	Low	Low
Manufacturability	High	Low	Low

FUTURE DIRECTIONS

Further testing is needed to fully realize the whole performance characteristics of these next generation sensors. The most important test to be performed is radiation testing. The QIS especially needs to be analyzed for radiation hardness since it has the most unique and least studied topology (initial tests are being studied by RIT and presented at this conference). Since it is a standard CMOS process, it should not be substantially different from pinned photodiode-based cameras; however, the vertical nature of the very small pixels has potential to alter its performance.

Other additional work that should be done is trying to bring Skipper or other novel readout technique to the various cameras to further improve performance. There is no fundamental reason why Skipper readout needs to be limited to improve only standard camera technologies. Having a more performant readout methodology has the potential to relax requirements in other parts of the camera chip. This could offer compounding levels of performance improvement.

CONCLUSION

In conclusion, the future of astronomical imaging is being shaped by innovative advancements in sensor technologies such as QIS, SPAD, and EMCCD cameras. Each brings unique strengths to the table: QIS with its low power and fast time resolution, SPAD with its precise timing, and EMCCD with its linearity, familiarity, and historical use. Overall, it is likely that single photon-counting sensors will quickly become an important cornerstone of space technologies. They will enable discoveries that have the potential to profoundly change our understanding of the universe. As technology progresses, these sensors will continue to play a critical role in pushing the frontiers of space exploration and scientific discovery.

ACKNOWLEDGMENTS

This work was supported by the National Science Foundation Research Traineeship, Transformative Research and Graduate Education in Sensor Science, Technology and Innovation (DGE- 2125733). A portion of this research, including support of a JPL internship for N.S., was carried out at the Jet Propulsion Laboratory, California Institute of Technology, under a contract with the National Aeronautics and Space Administration (80NM0018D0004).

REFERENCES

[1] P. Seitz and A. Theuwissen, Single-photon imaging, Springer Series in Optial Sciences, 2011.

[2] J. Ma, S. Chan and E. R. Fossum, "Review of Quanta Image Sensors for Ultralow-Light Imaging," *IEEE Transactions on Electron Devices,* vol. 69, no. 6, pp. 2824-2839, June 2022, doi: 10.1109/TED.2022.3166716.

[3] R. P. Mirin, S. W. Nam and M. A. Itzler, "Single-Photon and Photon-Number-Resolving Detectors," *IEEE Photonics Journal,* vol. 4, no. 2, pp. 629-632, April 2012, doi: 10.1109/JPHOT.2012.2190394.

[4] A. Suess, M. Wilhelmsen, L. Zuo and B. Fowler, "Time Domain Noise Analysis of Oversampled CMOS Image," *IEEE Transactions on Electron Devices,* vol. 69, no. 6, pp. 2973-2978, June 2022, doi: 10.1109/TED.2022.3169453.

[5] National Academies of Sciences, Engineering, and Medicine, Pathways to Discovery in Astronomy and Astrophysics for the 2020s, Washington, DC: The National Academies Press, 2023.

[6] S. Nikzad, M. E. Hoenk, J. Hennessy, A. D. Jewell, A. G. Carver, T. J. Jones, S. L. Cheng, T. Goodsall and C. Shapiro, "High performance silicon imaging arrays for cosmology, planetary sciences, & other applications," in *2014 IEEE International Electron Devices Meeting*, San Francisco, CA, USA, 2014, doi: 10.1109/IEDM.2014.7047027.

[7] S. Nikzad, A. D. Jewell, M. E. Hoenk, T. J. Jones, J. Hennessy, T. M. Goodsall, A. G. Carver, C. Shapiro, S. R. Cheng, E. T. Hamden, G. Kyne, D. C. Martin, D. Schiminovich, P. Scowen, K. France, S. McCandliss and R. E. Lupu, "High-efficiency UV/optical/NIR detectors for large aperture telescopes and UV explorer missions: development of and field observations with delta-doped arrays," *J. Astron. Telesc. Instrum. Syst.,* vol. 3, no. 3, p. 036002, 2017, doi: 10.1117/1.JATIS.3.3.036002.

[8] P. Morrissey, N. Bush, M. Hoenk, G. Kyne, A. Lamborn and J. Letona, "Flight photon counting camera development for the Roman Space Telescope Coronagraph Instrument," in *SPIE 12680, Techniques and Instrumentation for Detection of Exoplanets XI*, 2023, doi: 10.1117/1.JATIS.9.1.01600.

[9] J. Handal and K. Fox, "NASA Selects New Instruments for Priority Artemis Science on Moon," NASA, [Online]. Available: https://www.nasa.gov/news-release/nasa-selects-new-instruments-for-priority-artemis-science-on-moon/. [Accessed August 2024].

[10] NASA-JPL, "SPHEREx: About the mission," NASA JPL, [Online]. Available: https://www.jpl.nasa.gov/missions/spherex. [Accessed August 2024].

[11] Dragonfly, "Dragonfly Spacecraft and Science Payload," Johns Hopkins APL, [Online]. Available: https://dragonfly.jhuapl.edu/What-Is-Dragonfly/Spacecraft-and-Science-Payload.php. [Accessed August 2024].

[12] ESA, "Ariel factsheet," ESA, [Online]. Available: https://www.esa.int/Science_Exploration/Space_Science/Ariel_factsheet. [Accessed August 2024].

[13] ESA, "Comet Interceptor Instrumentation," ESA, [Online]. Available: https://www.cometinterceptor.space/instrumentation.html. [Accessed August 2024].

[14] J. W. N. Los, M. Sidorova, B. Lopez-Rodriguez, P. Qualm, J. Chang, S. Steinhauer, V. Zwiller and I. E. Zadeh, "High-performance photon number resolving detectors for 850–950 nm wavelength range," *APL Photonics,* vol. 9, no. 6, 5 June 2024.

[15] J. Hynecek, "Impactron-A New Solid State Image Intensifier," *IEE Transaction on Electron Devices,* vol. 48, no. 10, pp. 2238-2241, 2001.

[16] K. B. W. Harpsøe, M. I. Andersen and P. Kjægaard, "Bayesian photon counting with electron-multiplying charge coupled devices (EMCCDs)," *A&A*, vol. 537, no. A50, 2012, doi: 10.1051/0004-6361/201117089.

[17] S. Burri, Y. Maruyama, X. Michalet, F. Regazzoni, C. Bruschini and E. Charbon, "Architecture and applications of a high resolution gated SPAD image sensor," *Optics express*, vol. 22, no. 14, pp. 17573-17589, 2014, doi: 10.1364/OE.22.017573.

[18] J. Ma and E. R. Fossum, "A Pump-Gate Jot Device With High Conversion Gain for a Quanta Image Sensor," *IEEE Journal of the Electron Devices Society*, vol. 3, no. 2, pp. 73-77, March 2015, doi: 10.1109/JEDS.2015.2390491.

[19] D. A. Starkey and E. R. Fossum, "A novel threshold calibration methodology for quanta image sensors (QIS)," in *Int. Image Sensor Workshop (IISW)*, 2019.

[20] J. R. Janesick, T. S. Elliott, A. Dingiziam, R. A. Bredthauer, C. E. Chandler, J. A. Westphal and J. E. Gunn, "New advancements in charge-couple device technology: subelectron noise in 4096 x 4096 pixel CCDs," in *Proc. SPIE 1242, Charge-Coupled Devices and Solid State Optical Sensors*, 1990, doi: 10.1117/12.19452.

[21] D. A. Starkey and E. R. Fossum, "Determining conversion gain and read noise using a photon-counting histogram," *IEEE Journal of the Electron Devices Society*, vol. 4, no. 3, pp. 129-135, May 2016, doi: 10.1109/JEDS.2016.2536719.

[22] A. D. Jewell, C. Basset, S. Nikzad, G. Kyne, Y. Maruyama, N. Bush, J. Hennessy, T. J. Jones, M. Klein, S. Monacos, R. E. Rodriguez, D. Ardila, J. Bowman, J. Gamaunt, D. Gregory and D. Jacobs, "Performance of the SPARCS UV camera and detectors," in *SPIE 13093, Space Telescopes and Instrumentation 2024: Ultraviolet to Gamma Ray*, 2024, doi: 10.1117/12.3018492.

[23] O. E. Setälä, M. J. Prest, K. D. Stefanov, D. Jordan, M. R. Soman, V. Vähänissi and H. Savin, "CMOS Image Sensor for Broad Spectral Range with> 90% Quantum Efficiency," *Small*, vol. 19, no. 47, p. 2304001, 2023, DOI: 10.1002/smll.202304001.

[24] E. T. Hamden, A. D. J. C. A. Shapiro, S. R. Cheng, T. M. Goodsall, J. Hennessy, M. Hoenk, T. Jones, S. Gordon, H. R. Ong, D. Schiminovich, D. C. Martin and S. Nikzad, "Charge-coupled devices detectors with high quantum efficiency at UV wavelengths," *Journal of Astronomical Telescopes, Instruments, and Systems*, vol. 2, no. 3, p. 036003, 2016, doi: 10.1117/1.JATIS.2.3.036003.

[25] A. Ulku, C. Bruschini, X. Michalet, S. Weiss and E. Charbon, "A 512×512 SPAD image sensor with built-in gating," in *Int. Image Sensor Workshop*, Hiroshima, 2017.

[26] N. Teranishi, "Require Conditions for Photon-Counting Image Sensors," *IEEE Transactions on Electron Devices*, vol. 59, no. 8, pp. 2199-2205, 2012, doi: 10.1109/TED.2012.2200487.

[27] E. R. Fossum, "Modeling the Performance of Single-Bit and Multi-Bit Quanta Image Sensors," *IEEE Journal of the Electron Devices Society*, vol. 1, no. 9, pp. 166-174, 2013, doi: 10.1109/JEDS.2013.2284054.

[28] D. Robledo, "Photon-Counting CMOS Sensors Extend Frontiers in Scientific Imaging," Photonics Spectra, [Online]. Available: https://www.photonics.com/Articles/Photon-Counting_CMOS_Sensors_Extend_Frontiers_in/a67740. [Accessed August 2024].

[29] M, Wahl, "Time-Correlated Single Photon Counting," [Online]. Available: https://www.picoquant.com/images/uploads/page/files/7253/technote_tcspc.pdf.

[30] J. Ma, D. Zhang, D. Robeldo, L. Anzagira and S. Masoodian, "Ultra-high-resolution quanta image sensor with reliable photon-number-resolving and high dynamic range capabilities," *Sci Rep*, vol. 12, no. 13869, 2022, doi: 10.1038/s41598-022-17952-z.

[31] F. Piron, D. Morrison, M. R. Yuce and J. -M. Redouté, "A Review of Single-Photon Avalanche Diode Time-of-Flight Imaging Sensor Arrays," *IEEE Sensors Journal*, vol. 21, no. 11, pp. 12654-12666, 1 June 2021, doi: 10.1109/JSEN.2020.3039362.